

Article

Transient Luminous Events in the Lower Part of the Atmosphere Originated in the Peripheral Regions of a Thunderstorm

Ashot Chilingarian ^{1,*}, Gagik Hovsepyan ¹, Tigran Karapetyan ¹, Balabek Sargsyan ¹ and Ekaterina Svechnikova ²¹ Yerevan Physics Institute, Alikhanyan Brothers 2, Yerevan 0036, Armenia² Institute of Applied Physics of the RAS, 46 Ul'yanov Str., 603950 Nizhny Novgorod, Russia

* Correspondence: chili@aragats.am

Abstract: We present and discuss transient luminous events (TLEs) in the lower atmosphere, observed during large disturbances of the near-surface electric fields (NSEF) and coinciding with large enhancements of the particle fluxes (thunderstorm ground enhancements—TGEs). Despite large distances from the strongest electric field region, the maximum energy of TGE particles on 22 and 25 May 2018 reaches ≈ 40 MeV. Thus, the accelerating electric field reaches ≈ 2.0 keV/cm far from the zone of the strong lightning activity on the periphery of the storm. Light glows appearing simultaneously in the skies may be due to the local charge rearrangement generating a small illuminating discharge without initiating the lightning flash. This type of charge rearrangement does not lower the potential difference in the cloud, allowing the electron accelerator to operate and send particle fluxes in the direction of the earth's surface.

Keywords: RREA; TGE; TLE; NSEF; thunderstorm; energy spectrum; particle detectors

Citation: Chilingarian, A.; Hovsepyan, G.; Karapetyan, T.; Sargsyan, B.; Svechnikova, E. Transient Luminous Events in the Lower Part of the Atmosphere Originated in the Peripheral Regions of a Thunderstorm. *Universe* **2022**, *8*, 412. <https://doi.org/10.3390/universe8080412>

Academic Editor: Shuanggen Jin

Received: 17 May 2022

Accepted: 30 July 2022

Published: 5 August 2022

Publisher's Note: MDPI stays neutral with regard to jurisdictional claims in published maps and institutional affiliations.



Copyright: © 2022 by the authors. Licensee MDPI, Basel, Switzerland. This article is an open access article distributed under the terms and conditions of the Creative Commons Attribution (CC BY) license (<https://creativecommons.org/licenses/by/4.0/>).

1. Introduction

Thunderstorm ground enhancement (TGE, [1,2]), observed mostly in high mountain areas by a variety of particle detectors, is a large impulsive enhancement of electrons and gamma rays (rarely also neutrons [3,4]), lasting from tens of seconds to tens of minutes, sometimes exceeding the cosmic ray background hundreds of times [5]. These enhancements imply that very specific conditions of the atmospheric electric field are established, leading to the acceleration and multiplication of electrons [6]. The essence of these conditions is the emergence of an electrical dipole, which accelerates electrons in the direction of the ground and simultaneously decelerates positrons and muons [7]. Another dipole, operated in the upper part of the thundercloud, accelerates electrons in the direction of the open space. A few bremsstrahlung gamma rays emitted by these electrons are occasionally registered by the orbiting gamma ray observatories, called terrestrial gamma flashes (TGFs, [8]). The operation of both accelerators is triggered by the atmospheric electric field if the field exceeds the critical value, which equals $2.84 \text{ kV/cm} \times n$, where n is the density of air with respect to that at sea level [9–12]. Abundant at each height in the atmosphere, secondary electrons from small and large extensive air showers (EASs) serve as seeds for the relativistic runaway electron avalanches (RREAs) [13–15]. Additionally, the large EAS cores hitting the particle detectors can initiate millisecond duration bursts (“inverse TGFs” [16]). Both TGEs and TGFs are precursors of lightning flashes [17,18], helping to understand how lightning originates in the terrestrial atmosphere. The largest atmospheric electric field strength, measured in balloon flights [19], is much lower than needed for the conventional breakdown ($\approx 20 \text{ kV/cm}$, [20]). The possible scenarios of the RREA process, which initiates large TGEs are discussed in [21]. Comparison of measured

TGEs and simulations with GEANT4 [22] and CORSIKA [23] codes allow one to outline the plausible vertical profile of the electric field necessary for starting a runaway process.

Research in the past two decades has identified a surprising variety of “Transient Luminous Events” (TLEs) in the upper atmosphere and ionosphere, which accompany thunderstorms. Following the trend to look for the possible optical counterparts of thunderstorms, we establish on Aragats 24/7 monitoring of the skies by panoramic cameras as part of the multisensory research in high-energy atmospheric physics in attempts to find TLEs now in the lower atmosphere. In recent years, we registered a wide range of light structures, like large blobs in the center of the field of view (FoV) of the camera, near-vertical luminous filaments, narrow jets reaching the ground, and multiple small blobs covering almost the entire FoV of the panoramic camera. The predominant color of the light glows is blue-violet. To understand a new optical phenomenon in the lower atmosphere, we correlate the optical observations with measured electric field structures and particle fluxes. We perform detailed measurements of TGEs and disturbances of the near-surface electric field (NSEF) simultaneously with registering light glows. The sky monitoring system allows for the storage of numerous 1minute time series, which demonstrated appearing lightning flashes, light glows, birds, and precipitations.

We discovered that the optical flashes were not isolated events, but happened during active thunderstorms on the periphery of the strong lightning activity, usually accompanied by TGEs and special types of disturbances of NSEF. Peripheral storm regions do not produce lightning flashes, and instead, produce enigmatic light glows.

Measurements of TGEs at the periphery of the thunderstorm also provide clues to understanding the horizontal extension of the electric field, which supports RREA development in large areas. The size of the particle-emitting region in a thundercloud remains not well researched. Measurements with multiple dosimeters installed at nuclear power plants in a coastal area of the Japanese sea made it possible to follow the source of the gamma ray flux moving with an ambient wind flow [24]. At Nor Amberd Research Station, located on slopes of the Mt. Aragats at 2000 m height, the size of the particle emitting region was estimated using the muon stopping effect [25,26]. In both studies, the size of emitting regions is estimated to be about 1 km. However, in the recent radar-based gamma glow (TGE) study along the coast of the Japanese sea, it was observed that all TGEs were accompanied by the graupel fall, indicating the low location of the lower positively charged region [27]. A strong radar echo due to the high reflectivity of hydrometeors indicates that the vertical and horizontal extent of the strong accelerating electric field was larger than 2 km. In another observation of the gamma glow in Japan, the flux enhancements were initiated and terminated exactly at the same time at a distance of 1.35 km [28]. Thus, the size of the particle emitting region was previously highly underestimated.

We use facilities of the Aragats research station operated by cosmic ray division (CRD) of the Yerevan Physics Institute, i.e., networks of particle detectors, near-surface electric field (NSEF) sensors, lightning locators, and panoramic cameras, to relate the light glows to the special conditions of the electrified atmosphere, and to estimate the size of the particle emitting region using a large collection of TGEs registered on Aragats during last decade.

The structure of the paper is as follows. In the second section, we present networks of particle detectors and electric field sensors and explain data acquisition and time synchronization issues. In the third section, we provide the map of the thunderstorm development by the coordinates of lightning flashes, examples of the light glows, count rates of STAND1 particle detectors, their correlations plots, and TGE particle energy spectra. The relations between the light glows and disturbances of the NSEF are portrayed and discussed. Weather conditions and the method of cloud base height estimation are presented, and we also portray the charge structure of the lower dipole accelerating the electrons downward in direction of Earth’s surface. We also portray the picture of the location of lightning sensors, electric field sensors, and panoramic cameras to help readers achieve a full understanding of the experiment installations. The fourth section is devoted to the

correlation analysis of particle fluxes, light glows, and NSEF structures measured by different detectors and sensors. In conclusion, we present the summary figures outlining the peculiarities of the NSEF disturbances and the distribution of the distances to lightning flashes measured during the air glows. Comparisons with the analogical parameters of the TGE events not accompanied with glows are discussed.

2. Instrumentation

In Figure 1 we demonstrate the location of the two main networks used in this study. In Figure 1a we depict the Google map with located EFM 100 electric mills produced by the BOLTEK firm, widely used in atmospheric physics research. The EFM 100 sensors are operational at distances not larger than 33 km, with a response time of the instrument of ≈ 100 ms. EFM-100 electric mills measure NSEF with a frequency of 20 Hz and send measurements via WIFI to online computers, and then to the CRD's MySQL database. Usually, we use 1s averaged time series of the NSEF for the multivariate visualization and correlation analysis. We locate electric field sensors on masts due to deep snow in the winter months. The mast heights on which the electric field sensors are located vary from 3 to 13 m above the ground. The EFM 100 sensor also estimates the distance to the lightning flash within 33 km from the sensor with an accuracy of ≈ 1.5 km. The comparisons with WWLLN estimates of the distance to lightning from the station indicate a good agreement within the accuracies of both lightning location systems [29].

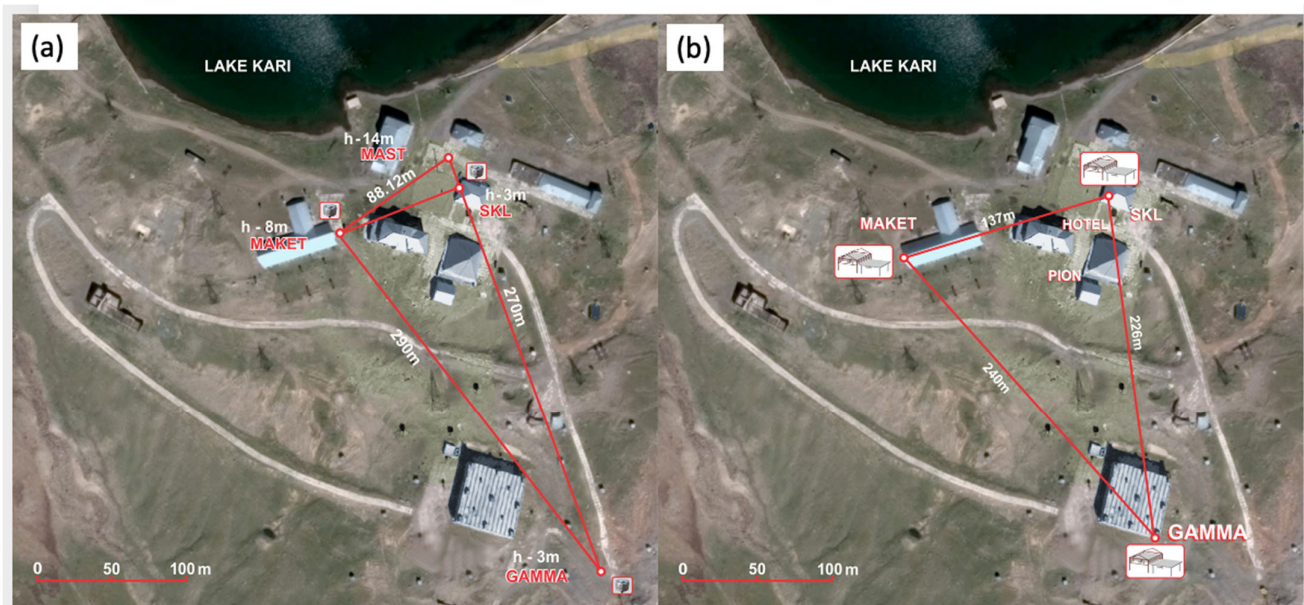


Figure 1. (a) EFM 100 electric mills network, near 4 sites the heights of masts are indicated; (b) STAND1 particle detector network.

In Figure 1b we portray the network of STAND1 particle detectors placed in the vertices of a triangle sides of which are equal to 133 m, 226 m, and 240 m. The “STAND1” detector is comprised of three layers of 1 cm thick, 1 m² sensitive-area scintillators stacked vertically and one 3 cm thick plastic scintillator of the same type stands apart. The light from the scintillator is reradiated into the long-wavelength region of the spectrum by the spectrum-shifter fibers and passed to the photomultiplier (PMT, FEU 115 M). The maximum luminescence is emitted at the 420 nm wavelength, with a luminescence time of about 2.3 ns [30]. The STAND1 detector is tuned by changing the high voltage applied to the PMT and by setting the thresholds for the shaper-discriminator. The discrimination level is chosen to guarantee both high efficiency of signal detection and maximal suppression of photomultiplier noise.

From simulations and from calibration experiments we estimate the efficiency of the STAND1 scintillators for charged particles as $\approx 95\%$. The energy thresholds of the upper, middle, and lower scintillators are 1, 5, and 8 MeV, respectively. The probability of registering a gamma ray by the upper, middle, and lower layers of the STAND1 detector are $\approx 2\%$, $\approx 2.5\%$, and $\approx 2.8\%$, respectively. Because of the very fast attenuation of TGE electrons in the atmosphere, the gamma ray flux usually is larger than the TGE electron flux 10–100 times, dependent on the height of the critical field above the ground. Using the energy spectrum of the TGE gamma rays and electrons recovered by the precise scintillation and NaI spectrometers, we reliably estimate the number of electrons and gamma rays registered in each of the 3 layers (see details in [31]).

The fast synchronized data acquisition (FSDAQ) provides registration of particle fluxes, and the near-surface electric field disturbances, harmonized with an accuracy of a millisecond. National Instrument's MyRio board (see Figure 2, [32]) includes eight analog inputs, four analog outputs, thirty-two digital I/O lines, FPGA, and a dual-core ARM Cortex-A9 processor, and GPS. With reconfigurable FPGA technology, we perform high-speed signal processing, high-speed control, inline signal processing, and custom timing and triggering. Eight digital inputs of three MyRio boards are used for feeding signals from the STAND1 network (four channels for each board, see Figure 2) and EFM 100 electric mill (by WiFi). Each of the three MyRio boards generates an output signal containing the 50 ms count rates registered by four scintillators, near-surface electric field value, and a GPS timestamp of the trigger signal. In this manner, the count rates and NSEF strengths measured by STAND1 and EFM 100 networks are synchronized on a millisecond time scale. The MyRio pulse-counting system can provide registration of very short time series (down to 1 ms) that enables the investigation of the dynamic of TGE development and its relation to the lightning initiation (50 ms time series are stored currently in the database). ADEI data analysis platform allows multivariate visualization and correlation analysis of the all-time series collected during 10 years of STAND1 network operation [33].

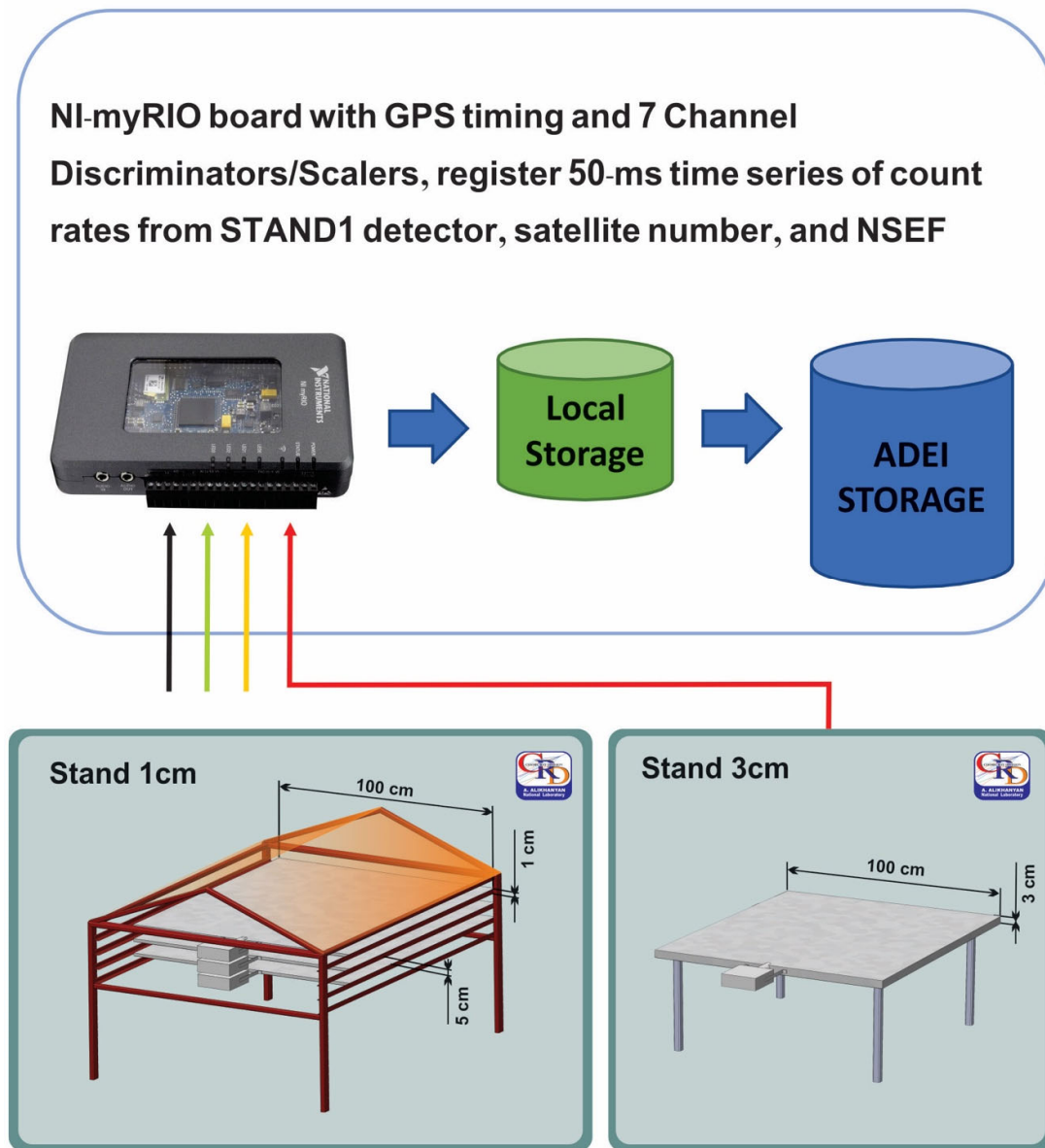


Figure 2. Fast data acquisition system for the STAND1 network units (three of the same type).

The structure of the atmosphere during TGE events was modeled using a numerical mesoscale model: the Weather Research and Forecasting Model [Advanced Research WRF (WRF-ARW), v. 4.1.2] [34]. The strategy of two nested domains is applied, with the center at the observation point (40.4715° , 44.1815°). The outer domain has dimensions of $2700 \times 1800 \text{ km}^2$ (the discretization step was 3 km), the inner domain with dimensions of $90 \times 90 \text{ km}^2$ (the discretization step is 1 km) covers the Aragats research station. The vertical coordinate in the inner domain has an irregular grid of 41 levels, the discretization changing from 50 m near the ground to 600 m at the height of 20 km. The WRF model includes various parameterizations describing physical processes on a sub-grid scale. The set of parameterizations providing the most reliable modeling for clouds producing TGE observed at the Aragats Station is based on the recommendations for fine meshes ($MP_PHYSICS = 8$, $RA_LW_PHYSICS = 4$, $RA_SW_PHYSICS = 4$, $RADT = 10$, $SF_SFCLAY_PHYSICS = 1$, $SF_SURFACE_PHYSICS = 2$, $BL_PBL_PHYSICS = 2$) and a verification procedure using the results of near-surface measurement, and satellite data [35].

3. Thundercloud Extension, Electric Field Strength and Particle Fluxes

The thundercloud coverage of Armenia, and particularly its presence above Aragats research station was estimated by the map of lightning locations with Boltek's storm tracker (lightning detection system [36]), powered by software from Astrogenics. Storm tracker defines four types of lightning discharges in radii up to 480 km around the location of its antenna: CG- (cloud-to-ground negative, lowering negative charge from the cloud to the ground), CG+ (cloud-to-ground positive, lowering positive charge to the ground), IC+ (normal polarity intracloud, lowering positive charge to the ground) and IC- (inverted polarity intracloud, lowering negative charge from the cloud to the ground).

By the examining time slices of the lightning activity, we determined from which direction the storm was coming, and, finally, by putting them on the map of all lightning occurrences we can observe that the storm's active zone missed the station (Figure 3).

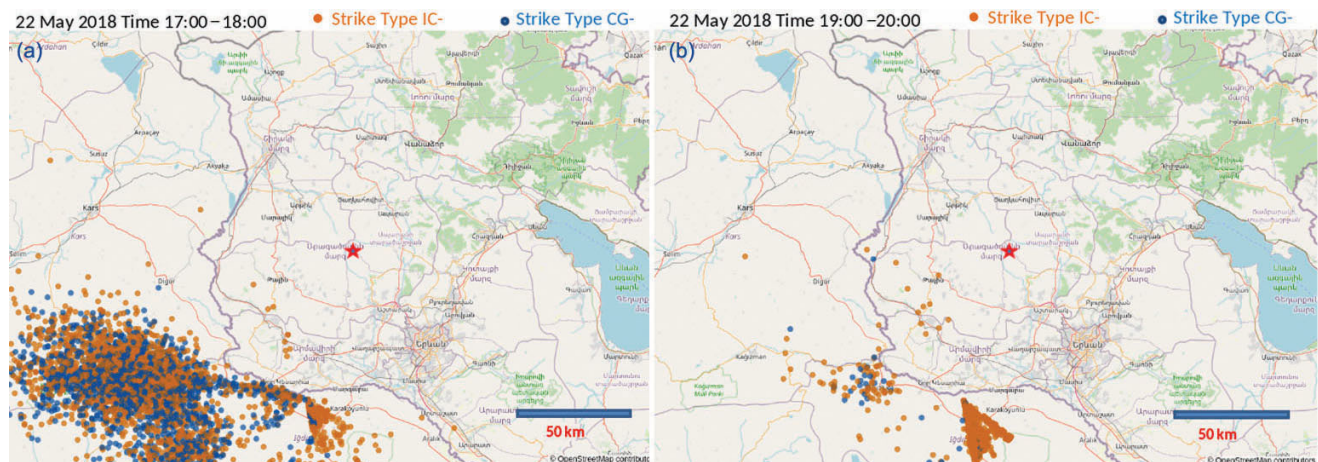


Figure 3. Map of lightning flashes obtained with Boltek's storm tracker on 22 May 2018, before TGE at 17:00–18:00 (a); and during TGE at 19:00–20:00 (b). The lightning type symbols and storm duration are portrayed in the upper panel, and the location of the Aragats research station is denoted by a red star.

In Figure 3, by mapping all flashes of a large storm coming from the southwest we demonstrate that the storm didn't approach the Aragats station on 22 May, and, therefore, TGE was not terminated by the lightning flash as usual, and continued for 18 min, as we can see in Figure 4e.

In Figure 4e we portray a 1s time series of three modules of the STAND1 network (upper 1 cm thick scintillators). The correlations between the MAKET-SKL detectors (Figure 4a, distance 88 m, correlation coefficient +0.81) are the same as the correlation between the MAKET-GAMMA detectors (Figure 4c, distance 240 m, correlation coefficient +0.82). There is no significant shift in the times of the maximum flux measured by detectors, as is indicated in Figure 4e. Delayed correlation plots (Figure 4b, 4d) are obtained by shifting time series one relative to another by 1 to 200 s. If there is a significant delay in particle arrivals, the maximum correlation will be shifted, and not peaked around the 0 value (within a few seconds). Thus, all 3 detectors demonstrate coherent time series of TGE count rates.

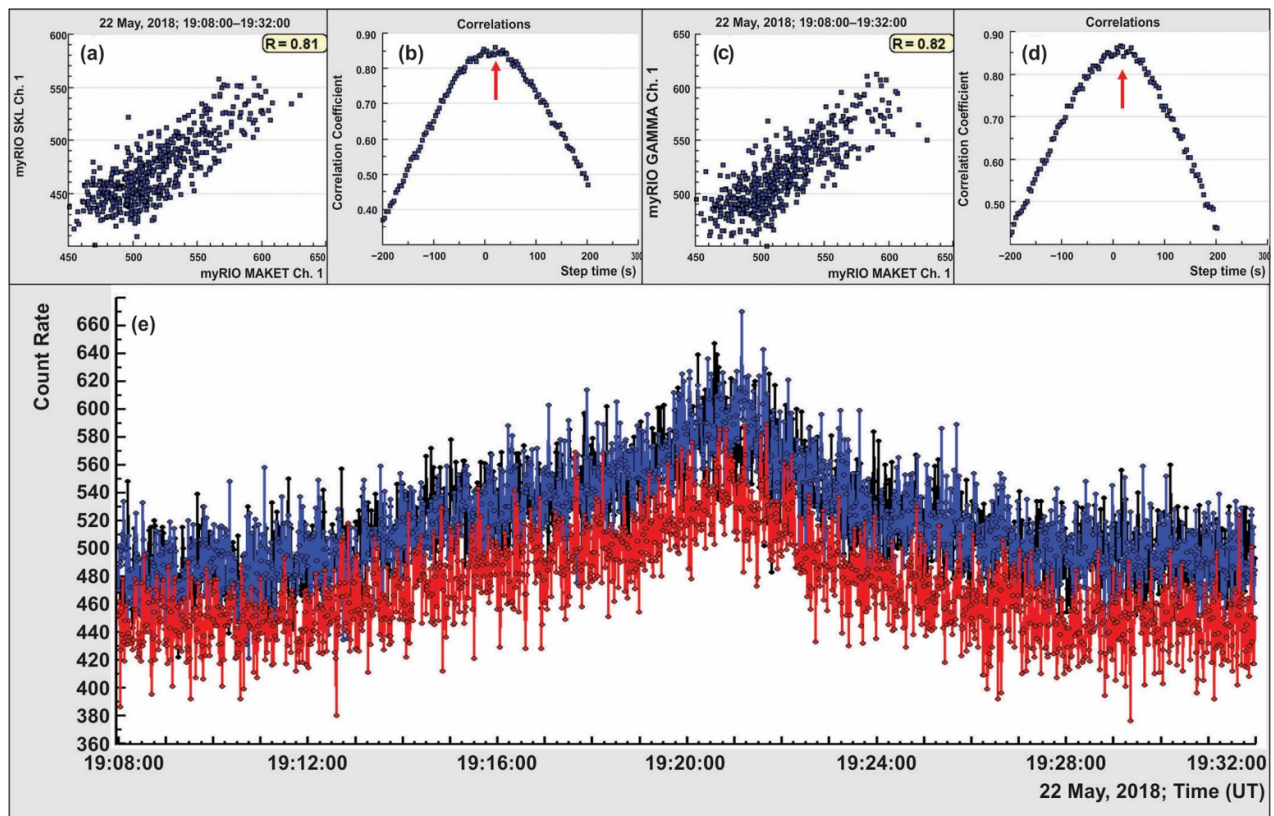


Figure 4. (a,b) scatter plots and delayed correlations plots (with a shift from -200 to 200 s) of count rates of STAND1 detector’s upper 1 cm thick scintillators (MAKET and SKL detectors); (c,d) the same for the MAKET and GAMMA detectors; (e) 1s time series of count rates of all three units of STAND1 network: MAKET (black), GAMMA (blue), and SKL (red). By red arrows we show the maximum correlation.

In Figure 5 we demonstrate the meteorological conditions observed during the TGE event. The outside temperature was $1.8\text{ }^{\circ}\text{C}$, and relative humidity was stable during TGE (95%); the cloud base was as low as 87.5 m for inset a), nearest lightning flash—on 10 km from the detectors, (see inset b). Cloud base height was estimated by calculating the spread between the air temperature and dew point according to the well-known approximate equation (see cloud base calculator [37]):

$$H(m) \approx (\text{Air temperature at surface } \{^{\circ}\text{C}\} - \text{dew point temperature } \{^{\circ}\text{C}\}) \times 125$$

As we can observe in Figure 5, despite the rainfall, the outside temperature and dew point were constant during TGE, thus, the height of the cloud base also was constant \approx at 90 m .

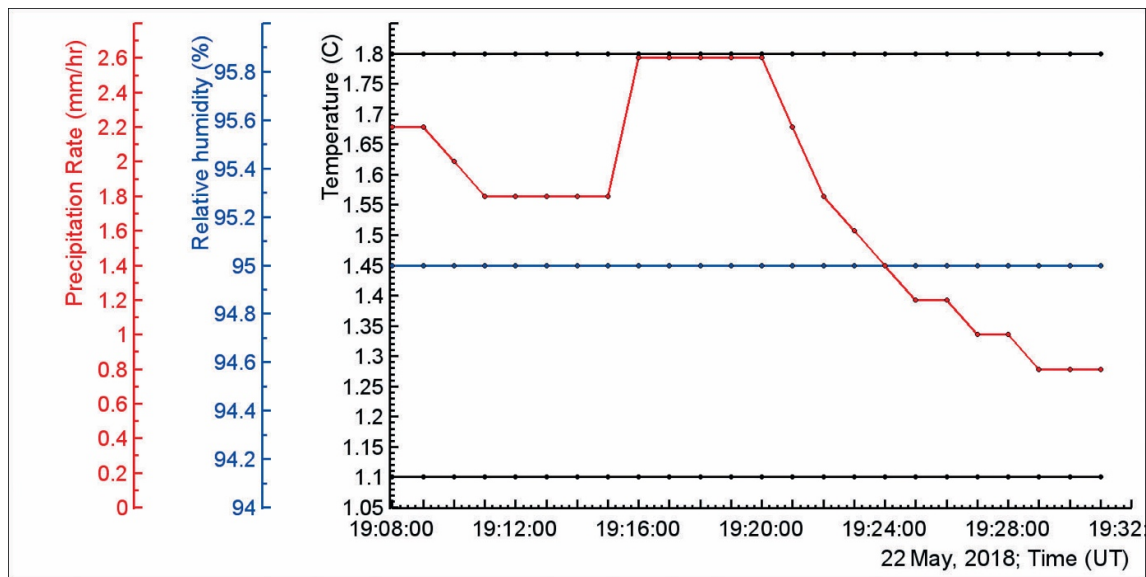


Figure 5. 1 min time series of outside temperature and dew point (black lines in the top and bottom); relative humidity (blue line in the middle); and rainfall (red line).

In Figure 6 we demonstrate the 1s time series of the NSEF, measured by the electric mill located on the roof of the MAKET experimental hall. NSEF was in the deep negative domain during TGE, with three outbursts of the NSEF with an amplitude of ≈ 10 kV/m occurring over 4 min (19:19–19:23), coinciding with TGE maximum flux (see Figure 4e). The time of the outburst occurrence coincides with the largest energies of the differential energy spectra registered by the network of NaI spectrometers at each minute of TGE (15–45 MeV), see Figure 7.

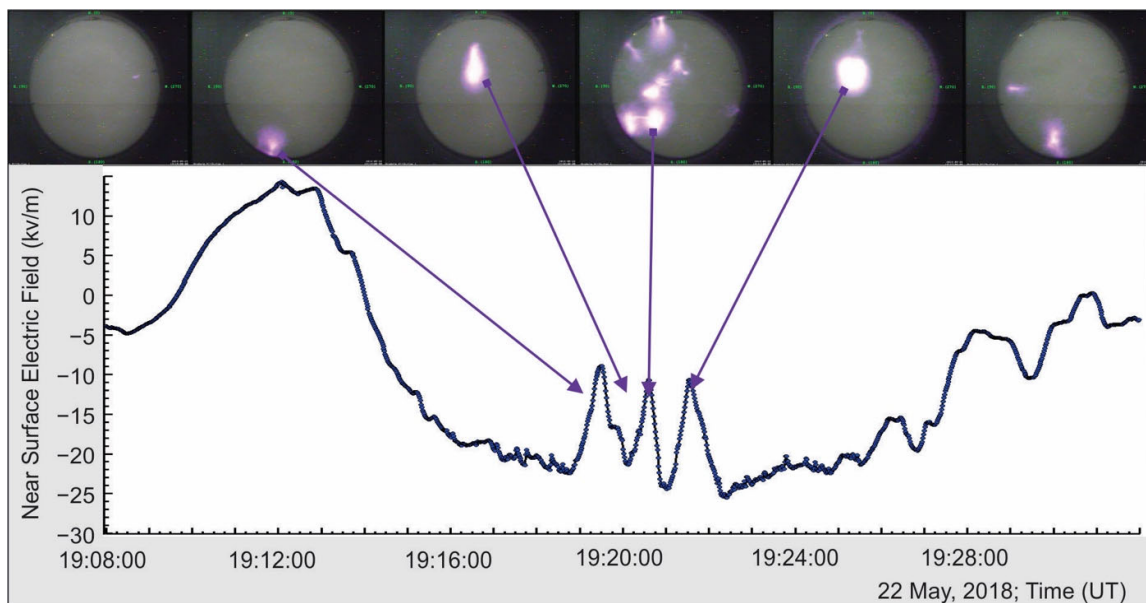


Figure 6. The disturbances of the NSEF during TGE, measured by an EFM 100 electric mill located on the roof of MAKET experimental hall (blue curve). In the upper panel, we demonstrate the 1-minute time series of the panoramic camera shots of the sky above the station, with a violet arrow we indicate the times when panoramic shots were done.

In the upper panel, we show the shots of the ALL SKY CAM panoramic camera, with intense violet lights that occurred during TGE. The light glows coincide with the NSEF outbursts and with the maximum of the TGE particle flux. The ALL SKY CAM model produced by Moonglow Technologies is a circular fisheye system providing 190° hemispherical field of view (FoV). The image sensor is a Color 1/3" Sony Super HAD CCD II with an effective pixel number across FoV is 546×457 , with automatic exposure time (from 10^{-5} to 4 s).

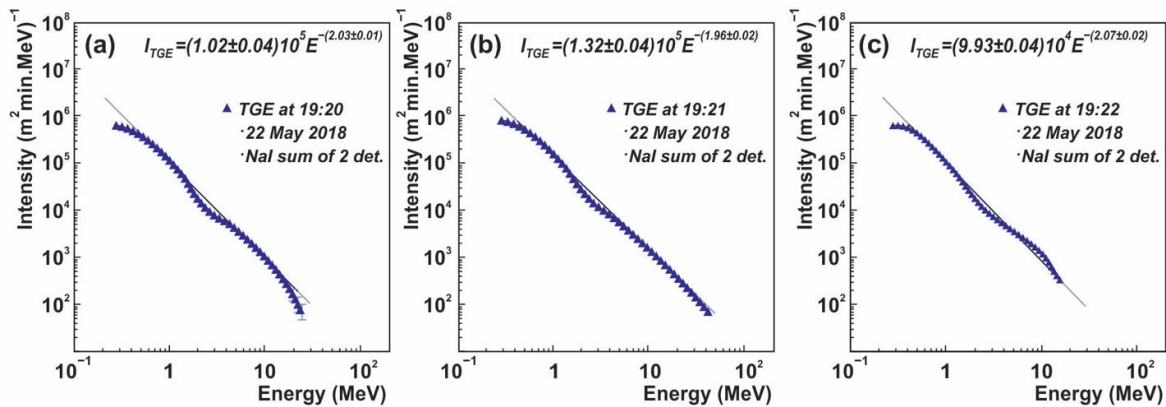


Figure 7. Differential energy spectra of TGE particles registered by NaI spectrometers at minutes of maximum flux.

In Figure 7 we demonstrate the differential energy spectra measured by the NaI spectrometers during minutes of the maximum flux. Seven NaI spectrometers are located under the roof of the MAKET experimental hall (0.7 mm of the iron tilts) and are monitoring the particle flux 24/7 [38]. Large sizes ($12 \times 12 \times 24$ cm) and low energy thresholds allow measurements of the energy spectra from 0.3 MeV up to 60 MeV. At the lower energies (less than 2 MeV) we can observe the contribution of the gamma radiation of ^{220}Rn progenies lifted to the atmosphere by NSEF [39]. The energy spectra above 3 MeV are due to TGE particles from the RREA avalanche reaching earth's surface. The maximum energy of the TGE particles, reaching 40 MeV, was measured at 19:19–19:21 (Figure 7b), in the middle of the disturbances of the NSEF, and when most of the light glows occurred (upper panel of Figure 6). Note that glows in the upper panel of Figure 6 coincide with the “outbursts” of NSEF, which lower the net negative charge above the ground. Thus, after each rearrangement of charge structure, the NSEF is impulsively enhanced and then returns to the previous value. This occurs three times.

In Figure 8 we portray light glows registered during the maximum of TGE flux only (there are much other light glows before and after TGE as well, posted in the Mendeleev dataset [40]). It is possible that the large particle fluxes and strong electric fields initiate discharges on high metallic masts around the Aragats station. However, we do not observe in Figure 8 any discharge on these structures (surrounded by red ovals).

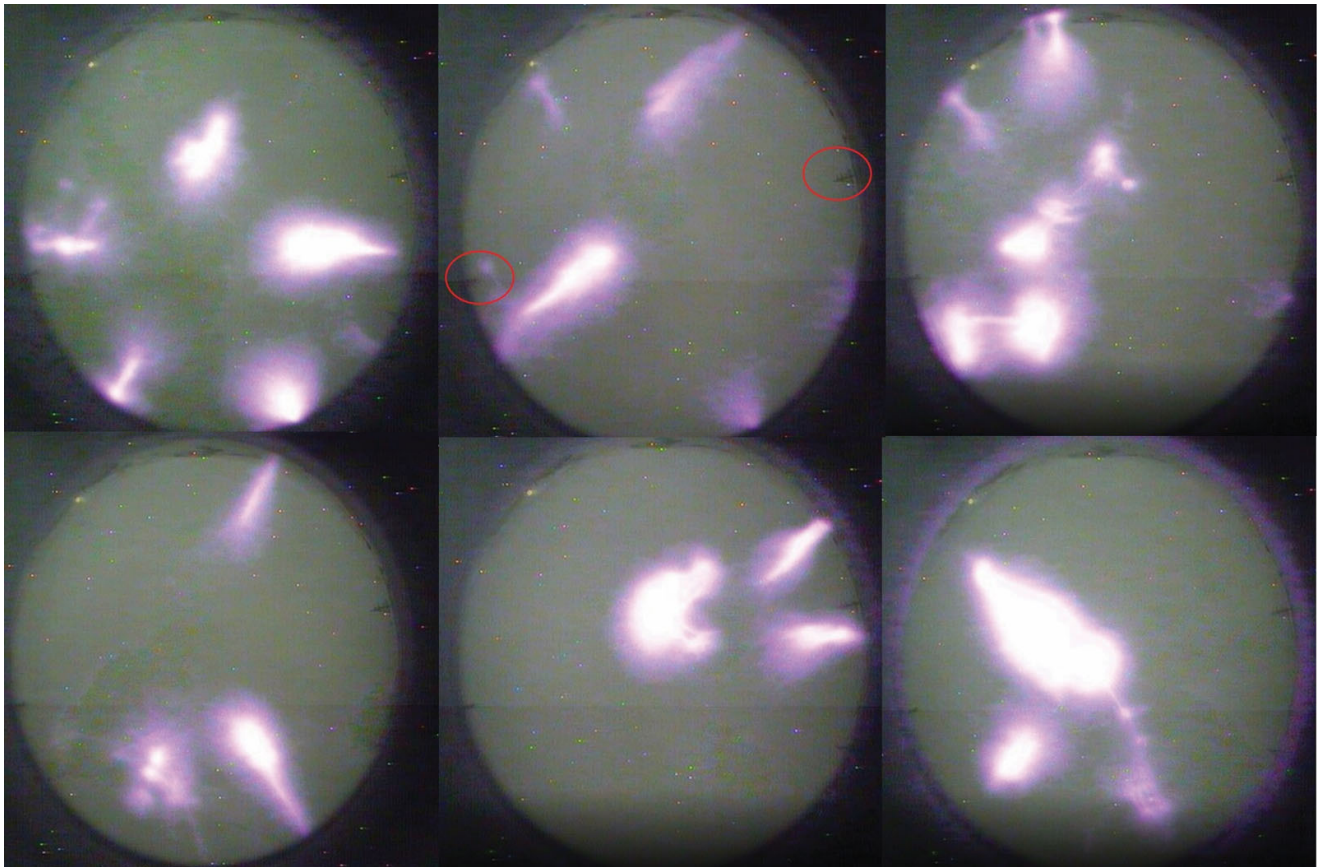


Figure 8. Selected light glows occurred during maximum minutes of TGE (19:19–19:21), the full collection available from the 1s clips [40]. With red ovals, we denote the two highest metallic structures on the station: the mast behind the MAKET experimental hall, and the chimney behind the hotel building, shown in Figure 9.

The panoramic camera is located on the mast above the roof of MAKET experimental hall (8 m height above the ground), thus only the highest masts enter the camera's field of view (FoV). The lights located at the edge of the FoV are connected to the earth's surface, however, there are many shots appearing in the center of FoV. The glows appeared in different locations in FoV, thus, the discharges appeared randomly in large regions of the sky below the clouds. In Figure 9, we portrayed the camera location on the roof of MAKET building and nearby metallic constructions, which can be sources of possible corona discharges. However, after installing additional cameras at 120 m from the first one, we see that the same glow (shifted from each other according to different FoV of cameras) appears in all three cameras, proving, that it is not a local corona discharge, but the sky glow. Additionally, we installed a "spy" camera observing the vicinity of the panoramic camera and it did not observe any corona discharge.



Figure 9. The MAKET experimental hall in winter, in the inset the zoomed ALL SKY CAM surrounded by DAVIS weather station, BOLTEK’s electric field sensor, and lightning tracker.

In the following pictures, we portray another very similar storm that occurred 3 days later; in the Mendeley dataset [40] we post exhaustive information on more than 10 similar storms accompanied with light glows; the summary histograms will be displayed in the discussion section.

We can observe in Figure 10 that a rather compact thunderstorm that occurred on 25 May 2018 approached from the southwest. The storm on 22 May, did not approach the Aragats station, and TGE continued for 14 min, as we can observe in Figure 11a and 11c. Thus, there was an offset of the storm active zone from the Aragats station, as we can observe in Figures 3 and 10. However, although the active lightning zone was rather far from the station, the electric field strength in the atmosphere was above the critical value of the runaway process, and an electron accelerator operates in the atmosphere for a few tens of minutes.

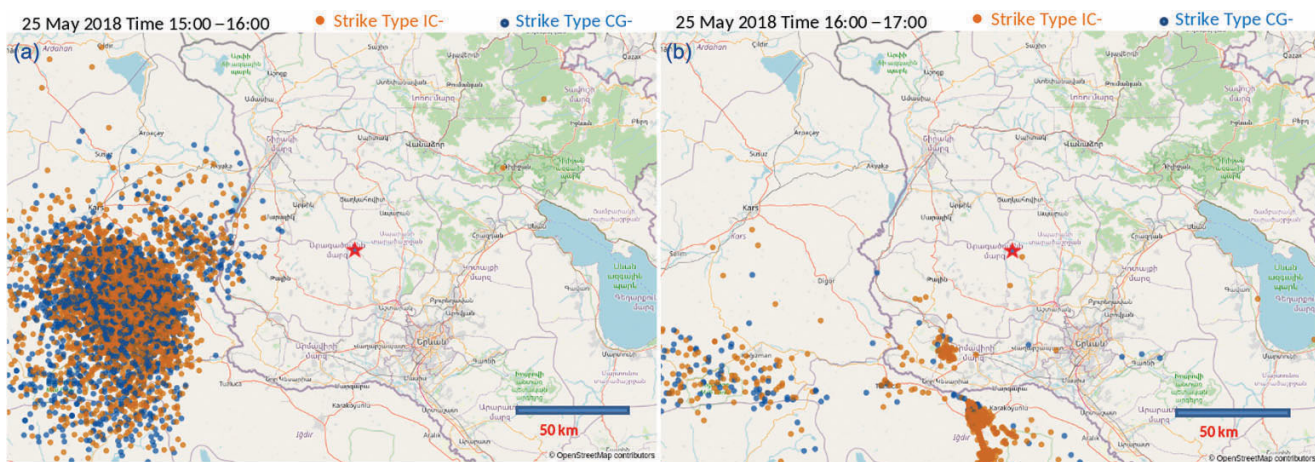


Figure 10. (a) Map of lightning flashes obtained with Boltek’s storm tracker on 25 May 2018, before the TGE at 15:00–16:00. The lightning type symbols and storm duration are portrayed in the upper panel, the Aragats research station location is indicated by a red star. (b): The “lightning” map observed just before and during TGE at 16:00–17:00 when the light glows appear above the station.

In Figure 11a we present 1s time series of three units of STAND1 network (stand-alone 3 cm thick scintillators, see Figure 2); all three count rates of STAND1 network precisely correlate.

It is interesting to see in Figure 11b that both the graupel (specks on the glass of the panoramic camera) and light glows occurred at the maximum of the TGE flux. The specific specks that appeared on the panoramic shots are connected with graupel fall, as we demonstrate as we demonstrate in [25], see Figures 11 and 12. In Figure 11c we portray a 1minute time series of the 3 cm thick scintillators belonging to the STAND3 detector (four stacked scintillators located in the SKL hall) along with disturbances of NSEF and remote lightning occurrences.

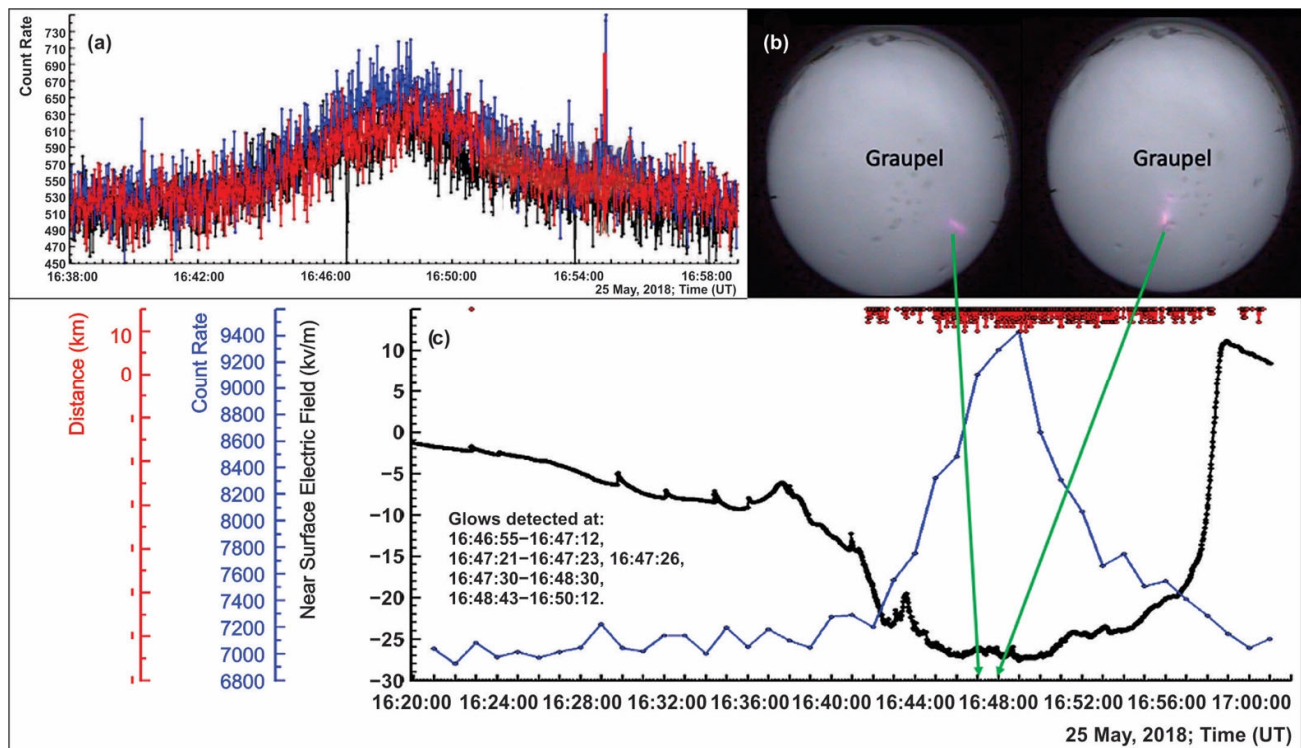


Figure 11. (a) Time series of 1 s count rates of 3 cm thick plastic scintillators of STAND1 network, MAKET (black), GAMMA (blue), and SKL (red); (b) panoramic camera shots with light spots and graupel fall specks observed at the maximum flux of TGE; (c) disturbances of the NSEF measured by EFM-100 sensor located nearby GAMMA surface array (black curve), 1minute time series of count rates of the 3 cm-thick plastic scintillator of STAND3 detector (energy threshold 4 MeV, blue curve), red lines in the upper part of the frame: remote lightning flashes. In the inset to frame (c) we indicate the times of glows; by green arrows, we denote the time of two glows that are portrayed in frame 11b).

In Figure 12 we demonstrate WRF modeling for the structure of the cloud revealing the snow (Figure 12b) and graupel (Figure 12a) clusters. The observed graupel fall and the lower cluster, which assumingly forms LPCR evidenced the emergence of the lower dipole that accelerated electrons in the direction of Earth’s surface. On 25 May, the density of the graupel cluster was relatively high; the graupel hydrometeors were located very low above the station. We assume that the modeled graupel cluster formed an LPCR, with which the snow cluster (the main-negative layer—MN) forms a lower dipole accelerating electrons in the direction of the earth’s surface. As we can observe in Figure 12, both clusters were in the same z-coordinates just above the station at the minutes of the maximum TGE flux and at the seconds when the light glows appear. Although the dipole MN-LPCR possibly plays a role in enhancing the electric field strength, the charge of the graupel

cluster was quite small (because the NSEF is deep negative), thus, we see that the predominant impact is caused by the negatively charged snow cluster. The graupel cluster is much closer to the surface than the upper snow cluster (about 10 times closer, which leads to a 100 times higher field for the same charge), and still, it does not create a field comparable with the field of the upper cluster. Therefore, we assume that the density of the graupel cluster is much smaller than the density of the snow cluster.

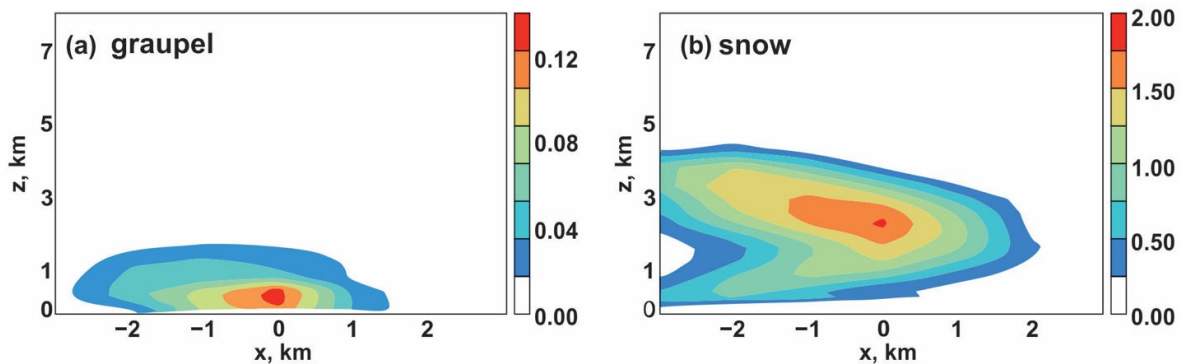


Figure 12. The spatial distribution of the graupel (a) and snow (b) particles modeled by WRF at 16:50 UT on 25 May 2018. The vertical axes started on Aragats station height (3200 m), x axes are oriented from west to east, and the coordinate origin (zero) corresponds to the location of the Aragats station. The coloring characterizes the density of hydrometeors in ng/cm^3 .

In Figure 13 we portray the 1s time series of the NSEF, measured by MAKET electric mill. During TGE, the NSEF was in the negative domain. In the upper panel, we portray the shots of the panoramic camera that continuously monitors the skies above the research station. The graupel fall indicates that a strong electric field can be extended below cloud base due to the falling positively charged graupels that oversee the electric field production. In contrast with the previous storm, which occurred on 22 May, the light glows are not so bright (see Figure 6), but considerably blurry. The height of the glows that are observed by panoramic cameras located on the ground is restricted by the cloud base height that scattered and absorbed the optical emissions. We surmise that lights are observed via a cloud that on 25 May was extremely low (25–60 m); on 22 May cloud base height was estimated to be ≈ 90 m, and lights were very bright, thus, we can estimate very roughly the height of the light glows to be 100 m.

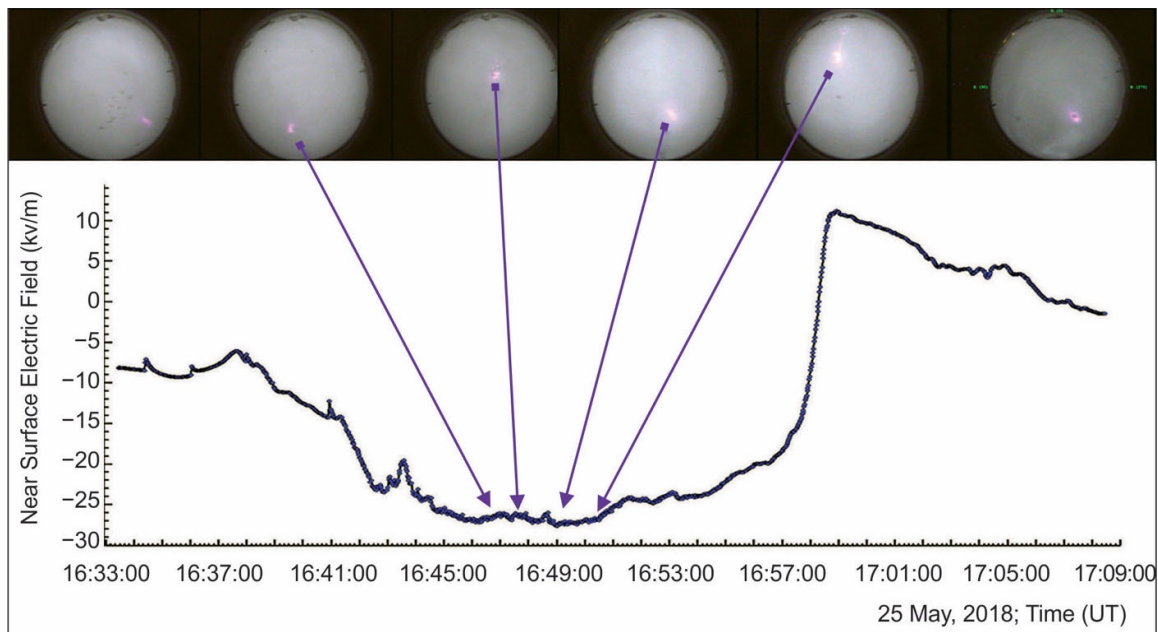


Figure 13. The disturbances of the NSEF during TGE, measured by EFM 100 electric mills located on the roof of MAKET experimental hall. In the upper panel we portray the panoramic camera shots of the sky above the station; with violet arrows, we indicate the times when panoramic shots were done.

4. Correlation Analysis of the Light Glows, NSEF Disturbances and Particle Fluxes

In this section, we will present the correlations of the light glows and NSEF in more detail to understand their possible origin. In Figure 14 we present the entire duration of a strong storm that occurred on 22 May 2018. The storm lasted nearly 4 hours, with multiple lightning flashes, and it passed aside from Aragats station (see Figure 3), however, initiated eight TGEs, two of which were significantly large (two largest peaks in Figure 14). All 8 TGEs occurred when NSEF was in a deep negative domain approaching -20 kV/m. In previous sections, we used only one NSEF sensor located on the roof of the MAKET experimental hall, but in this section, we will use data from all four electric field sensors to clarify the local effects of the charge rearrangements during TGE by using the delayed correlation techniques.

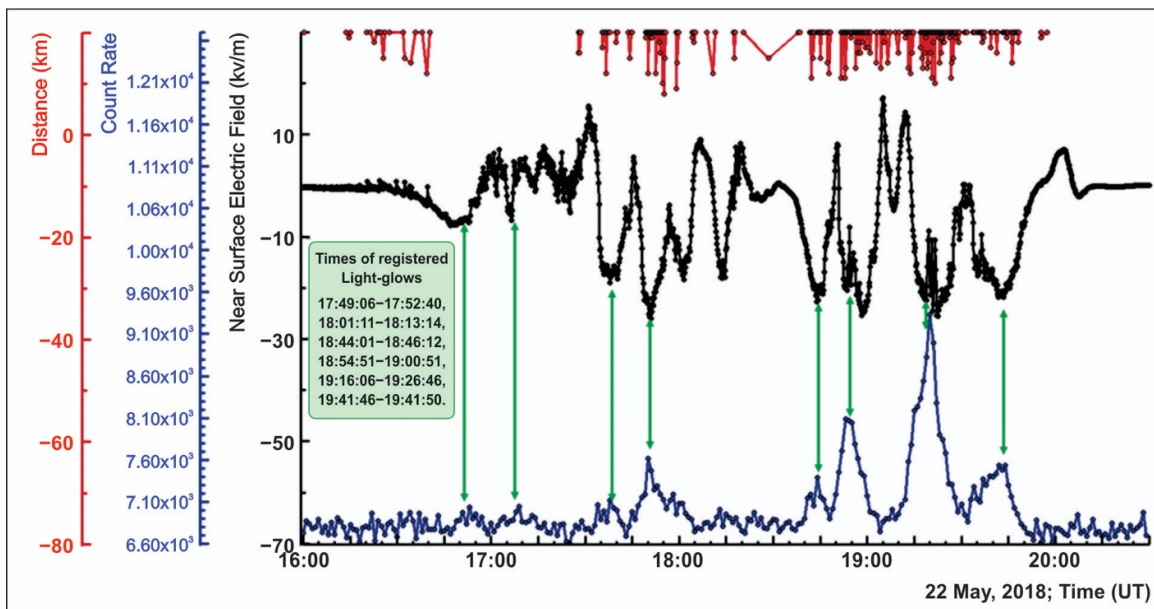


Figure 14. Disturbances of NSEF—black curve, 1minute count rate of the STAND3 particle detector with energy threshold ≈ 4 MeV—blue curve, distances to the lightning flashes—red lines. In inset—times of observed light glows. With green two-sided arrows, we connect TGEs with corresponding disturbances of NSEF.

In Figure 15 we portray the disturbances of NSEF measured by all four sensors of the network. We can see periodic and symmetric changes in the NSEF during the TGE. Three of the sensors located nearby on the highland demonstrate coherent peaks whose maximums coincide with an accuracy of a few seconds. The remote sensor located ≈ 300 m apart and ≈ 10 m lower in a valley exhibits two large peaks ahead of the other three and did not register the third peak.

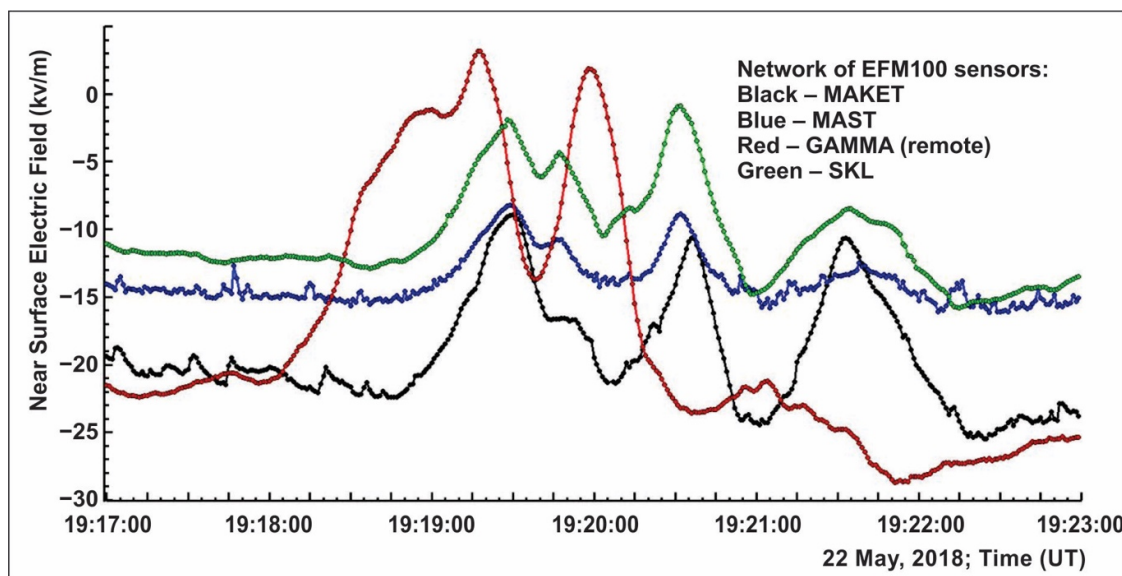


Figure 15. Disturbances of NSEF during 6 min of TGE registered by four electric field sensors of EFM 100 type.

In Figure 16 we present a detailed comparison of measurements made by two nearby electric field sensors, one on the MAKET experimental hall roof (black), and on the

standing alone 13 m high mast (blue). In the upper panel, we portray the scatter plot and delayed correlations plot presenting the precise coherence of both measurements (the bias of delayed correlation is near zero). In frames (c) and (d) we portray light glows, and in frame Figure 16g we outline the times of light glows with lines of different colors. Thus, we can relate the periodic changes of the NSEF with the appearance of light glows in the FoV of the panoramic camera. The difference in amplitudes of NSEF changes may be explained by the different locations of sensors. The sensor on the 13 m high mast is possibly not sensitive enough to the charge rearrangement aloft, compared to the sensor located 2 m above the metallic roof of the MAKET building.

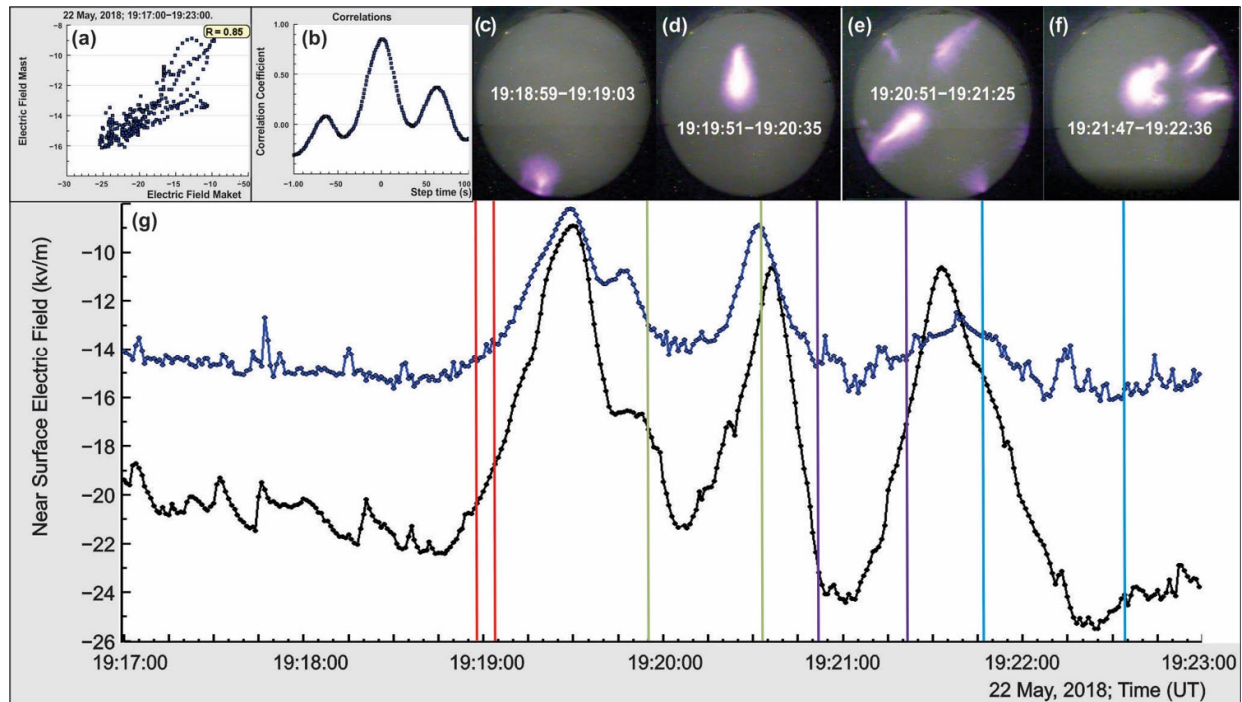


Figure 16. (g) 1s time series of NSEF disturbances measured by sensors located on the roof of MAKET building (black) and on the stand-alone 13 m high mast (blue). In the upper panel: (a) scatter plot of NSEF measurements, (b) the delayed correlations plot, (c–f) the patterns of registered light glows. Pairs of colored lines denote the times of registered glows correspondent to patterns portrayed above in frames (c–f).

In Figure 17 we portray the results of the correlation analysis of two remote NSEF sensors. From the delayed correlation plot we can observe the delay of the maximum correlation between electric field disturbances measured by the GAMMA EFM 100 located in a valley, and the same type device located on the roof of MAKET experimental hall. The correlation coefficient reaches a value of ≈ 0.7 when the time series of MAKET device is shifted by ≈ 30 s (see inset). The amplitude of field disturbances is also larger for GAMMA EFM. Thus, we can conclude that field rearrangement first influences the GAMMA sensor, and on the other 3 only after ≈ 30 s.

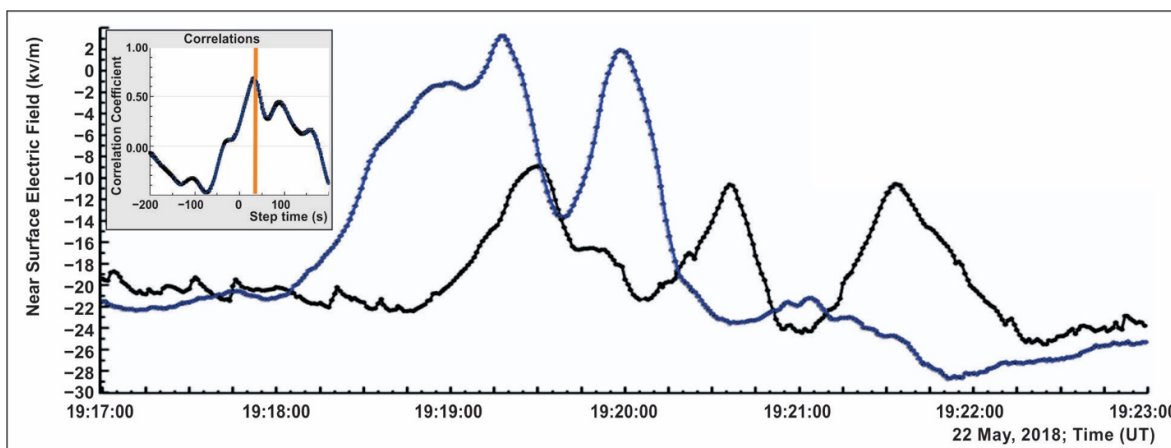


Figure 17. 1s time series of NSEF disturbances measured by electric field sensors located on the roof of MAKET building (black) and located above housing of GAMMA scintillators on 1 m high mast (blue). In inset — the delayed correlations plot.

The symmetric smooth shapes of analyzed NSEF disturbances are very different from the disturbances that originated from nearby lightning flashes. The nearby lightning discharges initiate the NSEF abrupt changes with the rise time of several hundreds of milliseconds and a long tail of tens of seconds. Highly symmetric and many-seconds-long periodic structures cannot be related to any of the lightning discharge. The disturbances portrayed in Figure 17 are not an exclusive case; in Figure 18 we present another symmetric structure registered during a significant TGE that occurred a few minutes before the analyzed one. Again, the time of the peak “outburst” measured by the GAMMA sensor is the same 30 s ahead of the MAKET sensor. However, the time amplitudes of both are equal.

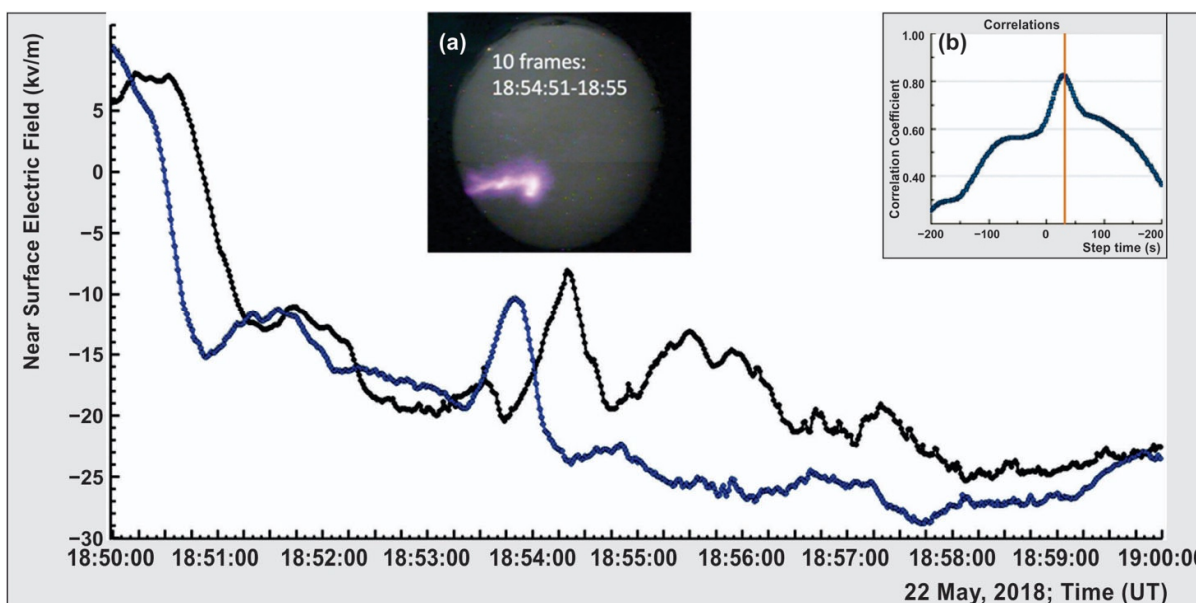


Figure 18. 1s time series of NSEF disturbances measured by sensors located on the roof of MAKET building (black) and located above housing of GAMMA scintillators on 1 m high mast (blue). In the inset (a)—the typical pattern of the light-glow, (b)—the delayed correlations plot.

5. Discussion and Conclusions

In our previous papers, we mentioned that TGEs are precursors of lightning flashes [17]. Recently we placed a collection of 165 TGEs in the Mendeley datasets, all terminated

by lightning flashes [41]. From this collection, supplied with links to explanatory materials, one can observe that the nearby flashes (distances less than 3 km) terminate the TGE just at the beginning of the rising phase; the middle-distance flashes (3–8 km) terminate at the maximum or on the TGE decaying phase.

Two TGEs described in this paper are very different from TGEs terminated by lightning flashes. Centers of the storm lightning activity were >10 km away from the detectors, and lightning flashes do not catastrophically lower the potential difference and do not abruptly terminate RREAs in the thunderous atmosphere above the particle detectors. Thus, particle fluxes continued for 14 and 18 min and are accompanied by light glows during the maximum flux of TGE. These considerably weak electrical discharges, that cause disturbances of the NSEF, do not trigger the Aragats system of electromagnetic pulse detection, which is triggered only by strong nearby lightning flashes. Lightning-active zones miss the station for both TGEs as is observed in the lightning location and WRF maps (Figures 3 and 10), and nearby lightning flashes occurred at distances of >10 km, do not terminate TGEs. The particle flux was stable at a ≈ 300 m scale, as we can observe from precisely correlated particle flux enhancements measured by remote detectors (see Figs 4 and 11). It indicates that the intracloud electric field that originates particle fluxes was stable on the minutes time scale. Thus, if the storm is just above particle detectors, nearby lightning flashes terminate RREA after a few minutes [42]. When the storm active zone is far from particle detectors (>10 km), the TGE extends for tens of minutes and smoothly terminates when conditions of the atmospheric electric field fail to support RREA. In Figure 19a, we portray the distribution of distances to lightning flashes abruptly terminated by the lightning flash. In Figure 19b we portray the same distribution for long-lasting TGEs, accompanied by light glows (a collection of these TGEs is posted in [40]). It is apparent that these distributions are belonging to distinct classes; only the second class (corresponding to the distribution presented in Figure 19b) mostly supports the origination of light glows.

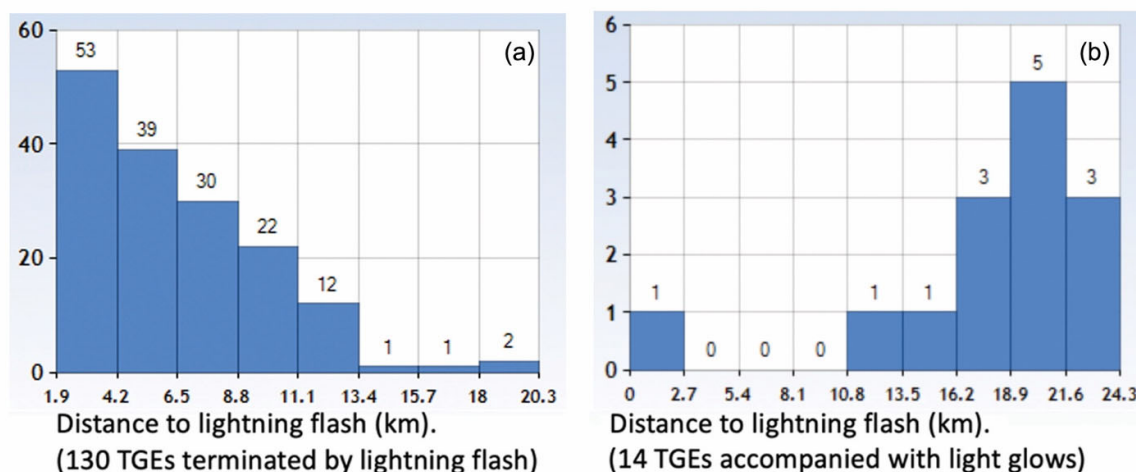


Figure 19. Distribution of the distances to the lightning flash for TGEs terminated by a flash (a), and for TGEs accompanied by the light glows (b).

Thus, the electron acceleration occurred in both cases and RREA particles covered large areas below thunderclouds. Therefore, the RREA can be unleashed in a very large spatial domain around the active lightning zone many kilometers apart.

Observed light glows are not local corona discharges on the camera mast, but a discharge in the atmosphere above the Aragats station, influencing all electric sensors. These discharges do not initiate lightning flash, only local disturbances of the NSEF and light glows in the sky above the station. The delay correlation analysis demonstrates that the

network of NSEF sensors registers a slightly different field disturbance due to the different orographic locations of the sensors.

During the most of glow events, the NSEF was in the deep negative domain, only 3 from 14 were in the positive domain, see Figure 20. The origin of light glows is under discussion; the possible explanations are intense fluxes of TGE electrons [43,44], ball lightning [45,46], St. Elmo's fires, and geomagnetic disturbances [47]. However, after examining luminous TGE events, along with lightning location maps and NSEF time series, we surmise that an electrical discharge much weaker than a lightning flash could only partially neutralize the charge above, and hence, only partially lower the corresponding potential difference, allowing the electron accelerator to operate and send particle fluxes in the direction of Earth's surface. Simultaneously, these types of discharges initiate light glows in the thunderous atmosphere.

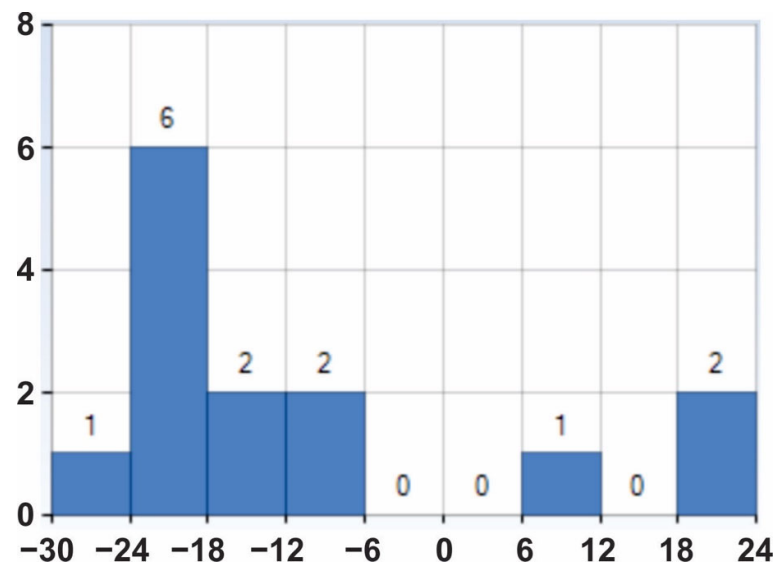


Figure 20. The NSEF strengths distribution for the TGE events accompanied by light glows.

Terrestrial gamma-ray flashes (TGFs) comprise very few high-energy photons from RREAs unleashed in the upper dipole, and occasionally reaching orbiting gamma observatories. They are associated with severe thunderstorms in the equatorial regions, however, due to the large distance from the source to spectrometers, located on the satellites, different scenarios of relative time-sequence of TGF and lightning are reported. Recently, the Atmosphere-Space Interactions Monitor (ASIM) consisting of X- and gamma-ray detectors, optical photometers, and cameras clarified the temporal relation between TGFs and lightning discharges. The authors of [18] conclude that TGFs precede lightning flashes. Thus, ASIM measurements evidenced that possibly lightning flashes do not originate MeV gamma rays, as was indicated already for TGEs [17]. Thus, now we have additional evidence of the analogical origin of TGEs and TGFs.

Additionally, ASIM photometers register an optical signal preceding the optical pulse associated with the lightning by a few milliseconds. A 300 km distance from photometers to thunderclouds does not allow to obtain a detailed time series of shots, however, the optical light registration during TGFs demonstrates the universality of the RREA process for both avalanches in the upper (TGF) and lower (TGE) dipoles in the thunderous atmosphere.

Author Contributions: A.C. was responsible for the Conceptualization, and supervision. He performs correlation analysis of the particle fluxes, light glows, and disturbances of the near-surface electric field. He wrote the manuscript. G.H. was responsible for the energy spectra recovery and analysis. T.K. was responsible for the uninterrupted operation of all facilities of the high-altitude

research station, and for validation of measurement results. B.S. was responsible for data curation, visualization, and installing of panoramic cameras and collecting and analyzing panoramic shots with light glows. E.S. was responsible for the modeling with WRF and recovering of the lower dipole charge structure. All authors have read and agreed to the published version of the manuscript.

Funding: This research received no external funding

Data Availability Statement: The data for this study are available in numerical and graphical formats on the WEB page of the Cosmic Ray Division (CRD) of the Yerevan Physics Institute, <http://adei.crd.yerphi.am/adei> and from Mendeley datasets [14,26] accessed on 31 January 2022

Acknowledgments: We thank the staff of the Aragats Space Environmental Center for the uninterrupted operation of experimental facilities on Aragats under severe weather conditions. The authors are thankful to Nikolay Ilin for the assistance in WRF modeling and discussing the results. The data for this study is available in numerical and graphical formats by the multivariate visualization software platform ADEI on the WEB page of the Cosmic Ray Division (CRD) of the Yerevan Physics Institute, <http://adei.crd.yerphi.am/adei> and from Mendeley datasets. E. Svechnikova appreciates the support of the IAPRAS Project No. 0030-2021-0028 in the analysis of the numerical model of the atmosphere. The authors acknowledge the support of the Science Committee of the Republic of Armenia (research project No 21AG- 1C012), in the modernization of the technical infrastructure of high-altitude stations.

Conflicts of Interest: The authors declare no conflict of interest.

References

- Chilingarian, A.; Daryan, A.; Arakelyan, K.; Hovhannisyanyan, A.; Mailyan, B.; Melkumyan, L.; Hovsepyan, G.; Chilingaryan, S.; Reymers, A.; Vanyan, L. Ground-based observations of thunderstorm-correlated fluxes of high-energy electrons, gamma rays, and neutrons. *Phys. Rev. D* **2010**, *82*, 043009.
- Chilingarian, A.; Hovsepyan, G.; Hovhannisyanyan, A. Particle bursts from thunderclouds: Natural particle accelerators above our heads. *Phys. Rev. D* **2011**, *83*, 062001.
- Chilingarian, A.; Bostanjyan, N.; Vanyan, L. Neutron bursts associated with thunderstorms. *Phys. Rev. D* **2012**, *85*, 085017.
- Chilingarian, A.; Bostanjyan, N.; Karapetyan, T.; Vanyan, L. Remarks on recent results on neutron production during thunderstorms. *Phys. Rev. D* **2012**, *86*, 093017.
- Chum, J.; Langer, R.; Baše, J.; Kollárik, M.; Strhárský, I.; Diendorfer, G.; Rusz, J. Significant Enhancements of Secondary Cosmic Rays and Electric Field at the High Mountain Peak of Lomnický Štít in High Tatras during Thunderstorms. *Earth Planets Space* **2020**, *72*, 28. <https://doi.org/10.1186/s40623-020-01155-9>.
- Chilingarian, A.; Hovsepyan, G.; Zazyan, M. Measurement of TGE particle energy spectra: An insight in the cloud charge structure. *Europhys. Lett.* **2021**, *134*, 6901. <https://doi.org/10.1209/0295-5075/ac0dfa>.
- Chilingarian, A.; Hovsepyan, G.; Zazyan, M. Muon tomography of charged structures in the atmospheric electric field. *Geophys. Res. Lett.* **2021**, *48*, e2021GL094594. <https://doi.org/10.1029/2021GL094594>.
- Fishman, G.J.; Bhat, P.N.; Mallozzi, R.; Horack, J.M.; Koshut, T.; Kouveliotou, C.; Pendleton, G.N.; Meegan, C.A.; Wilson, R.B.; Paciesas, W.S.; et al. Discovery of intense gamma ray flashes of atmospheric origin. *Science* **1994**, *264*, 1313.
- Roussel-Dupré, R.; Symbalisty, E.; Taranenko, Y.; Yukhimuk, V. Simulations of high-altitude discharges initiated by runaway breakdown. *J. Atmos. Sol.-Terr. Phys.* **1998**, *60*, 917–940.
- Dwyer, J.R. A fundamental limit on electric fields in air. *Geophys. Res. Lett.* **2003**, *30*, 2055.
- Babich, L.P.; Donskoy, E.N.; Il'kaev, R.I.; Kutsyk, I.M.; Roussel-Dupré, R.A. Fundamental parameters of a relativistic runaway electron avalanche in air. Plasma physics reports. *Plasma Phys. Rep.* **2004**, *30*, 616–624.
- Dwyer, J.R.; Smith, D.M.; Cummer, S.A. High-Energy Atmospheric Physics: Terrestrial Gamma-Ray Flashes and Related Phenomena. *Space Sci. Rev.* **2012**, *173*, 133–196. <https://doi.org/10.1007/s11214-012-9894-0>.
- Gurevich, A.V.; Milikh, G.M.; Roussel-Dupre, R. Runaway electron mechanism of air breakdown and preconditioning during a thunderstorm. *Phys. Lett. A.* **1992**, *165*, 463–468. [https://doi.org/10.1016/0375-9601\(92\)90348-P](https://doi.org/10.1016/0375-9601(92)90348-P).
- Babich, L.P.; Donskoy, E.N.; Kutsyk, I.M.; Kudryavtsev, A.Y.; Roussel-Dupre, R.A.; Shamraev, B.N.; Symbalisty, E.M. Comparison of relativistic runaway electron avalanche rates obtained from Monte Carlo simulations and kinetic equation solution. *IEEE Trans. Plasma Sci.* **2001**, *29*, 430–438. <https://doi.org/10.1109/27.928940>.
- Alexeenko V.V., Khaerdinov N.S., Lidvansky A.S. Petkov V.B. Transient variations of secondary cosmic rays due to atmospheric electric field and evidence for pre-lightning particle acceleration. *Physics Letters A.* **2002**; *301(3–4)*: 299–306. DOI:10.1016/S0375-9601(02)00981-7.
- Chilingarian, A.; Hovsepyan, G. The synergy of the cosmic ray and high energy atmospheric physics: Particle bursts observed by arrays of particle detectors. *New Astron.* **2022**, *97*, 101871.

17. Chilingarian, A.; Chilingaryan, S.; Karapetyan, T.; Kozliner, L.; Khanikyants, Y.; Hovsepyan, G.; Pokhsroryan, D.; Soghomonyan, S. On the initiation of lightning in thunderclouds. *Sci. Rep.* **2017**, *7*, 1371. <https://doi.org/10.1038/s41598-017-01288-0>.
18. Lindanger, A.; Skeie, C.A.; Marisaldi, M.; Bjørge-Engeland, I.; Østgaard, N.; Mezentssev, A.; Sarria, D.; Lehtinen, N.; Reglero, V.; Chanrion, O.; et al. Production of terrestrial gamma-ray flashes during the early stages of lightning flashes. *J. Geophys. Res. Atmos.* **2022**, *127*, e2021JD036305. <https://doi.org/10.1029/2021JD036305>.
19. Stolzenburg, M.; Marshall, T.C.; Rust, W.D.; Bruning, E.; MacGorman, D.R.; Hamlin, T. Electric field values observed near lightning flash initiations. *Geophys. Res. Lett.* **2007**, *34*, L04804.
20. Gurevich, A.V.; Zybin, K.P. Runaway Breakdown and the Mysteries of Lightning. *Phys. Today* **2005**, *58*, 37–43.
21. Chilingarian, A.; Hovsepyan, G.; Svechnikova, E.; Zazyan, M. Electrical structure of the thundercloud and operation of the electron accelerator inside it. *Astropart. Phys.* **2021**, *132*, 102615 <https://doi.org/10.1016/j.astropartphys.2021.102615>.
22. Agostinelli, S.; Allison, J.; Amako, K.A.; Apostolakis, J.; Araujo, H.; Arce, P.; Asai, M.; Axen, D.; Banerjee, S.; Barrand, G.J. GEANT4—A simulation toolkit. *Nucl. Instrum. Methods Phys. Res.* **2003**, *506*, 250.
23. Heck, D.; Knapp, J.; Capdevielle, J.N.; Schatz, G.; Thouw, T. Forschungszentrum, Karlsruhe, Report No. FZKA 6019. 1998. Available online: <https://www.ikp.kit.edu/corsika/70.php> (accessed on 1 January 2022).
24. Torii, T.; Sugita, T.; Kamogawa, M.; Watanabe, Y.; Kusunoki, K. Migrating source of energetic radiation generated by thunderstorm activity. *Geophys. Res. Lett.* **2011**, *38*, 24.
25. Chilingarian, A.; Hovsepyan, G.; Karapetyan, G.; Zazyan, M. Stopping muon effect and estimation of intracloud electric field. *Astropart. Phys.* **2021**, *124*, 102505.
26. Chilingarian, A.; Bostanjyan, N.; Karapetyan, T. On the possibility of location of radiation-emitting region in thundercloud. *IOP Publ. J. Phys. Conf. Ser.* **2013**, *409*, 012217. <https://doi.org/10.1088/1742-6596/409/1/012217>.
27. Wada, Y.; Enoto, T.; Kubo, M.; Nakazawa, K.; Shinoda, T.; Yonetoku, D.; Sawano, T.; Yuasa, T.; Ushio, T.; Sato, Y.; et al. Meteorological aspects of gamma-ray glows in winter thunderstorms. *Geophys. Res. Lett.* **2021**, *48*, e2020GL091910. <https://doi.org/10.1029/2020GL091910>.
28. Hisadomi, S.; Nakazawa, K.; Wada, Y.; Tsuji, Y.; Enoto, T.; Shinoda, T.; Morimoto, T.; Nakamura, Y.; Yuasa, T.; Tsuchiya, H. Multiple gamma-ray glows and a downward TGF observed from nearby thunderclouds. *J. Geophys. Res. Atmos.* **2021**, *126*, e2021JD034543.
29. Soghomonyan, S.; Chilingarian, A. Thunderstorm Ground Enhancements Abruptly Terminated by a Lightning Flash Registered Both by WWLLN and Local Network of EFM-100 Electric Mills. Mendeley Data, V1. 2021. Available online: <https://data.mendeley.com/datasets/ygvjzdx3w3/1> (accessed on 1 January 2022).
30. Britvich, G.I.; Chernichenko, S.K.; Chubenko, A.P.; Gilitsky, Y.V.; Kushnirenko, A.E.; Mamidzhanyan, E.A.; Pavlyuchenko, V.P.; Shein, I.V.; Soldatov, A.P.; Shepetov, A.L.; et al. The large scintillation charged particles detector of the Tien-Shan complex “ATHLET”. *Nucl. Instrum. Methods A* **2006**, *564*, 225–234.
31. Chilingarian, A.; Hovsepyan, G.; Karapetyan, T.; Sargsyan, B.; Chilingaryan, S. Measurements of energy spectra of relativistic electrons and gamma-rays avalanches developed in the thunderous atmosphere with Aragats Solar Neutron Telescope. *J. Instrum.* **2022**, *17*, P03002.
32. Pokhsroryan, D. Fast Data Acquisition system based on NI-myRio board with GPS time stamping capabilities for atmospheric electricity research, Proceedings of TEPA Symposium, Nor Amberd, Armenia, 5–9 October 2015; Tigran Mets: Yerevan, 2016; p. 23.
33. Chilingaryan, S.; Chilingarian, A.; Danielyan, V.; Eppler, W. The aragats data acquisition system for highly distributed particle detecting networks. *J. Phys. Conf. Ser.* **2008**, *119*, 082001.
34. Skamarock, W.C.; Klemp, J.B.; Dudhia, J.; Gill, D.O.; Liu, Z.; Berner, J.; Wang, W.; Powers, J.G.; Duda, M.G.; Barker, D.M.; et al. *A Description of the Advanced Research WRF Model Version 4*; National Center for Atmospheric Research: Boulder, CO, USA, 2019. <https://doi.org/10.5065/1dfh-6p97>.
35. Svechnikova, E.K.; Ilin, N.V.; Mareev, E.A.; Chilingarian, A.A. Characteristic features of the clouds producing thunderstorm ground enhancements. *JGR Atmos.* **2021**, *126*, e2019JD030895.
36. Available online: <https://www.boltek.com/product/ld350-long-range-detection-kit> (accessed on 1 March 2022).
37. Available online: <https://www.omnicalculator.com/physics/cloud-base> (accessed on 1 January 2022).
38. Chilingarian, S.; Chilingaryan, G.; Hovsepyan, G. Calibration of particle detectors using gamma-ray beams from thunderclouds. *Astropart. Phys.* **2015**, *69*, 37–43.
39. Chilingarian, A.; Hovsepyan, G.; Sargsyan, B. Circulation of Radon progeny in the terrestrial atmosphere during thunderstorms. *Geophys. Res. Lett.* **2020**, *47*, e2020GL091155. <https://doi.org/10.1029/2020GL091155>.
40. Chilingarian, A.; Hovsepyan, G.; Sargsyan, B. Catalog of Sky Glows above Aragats Mountain. Mendeley Data, V1. 2022. Available online: <https://data.mendeley.com/datasets/8ygy98r99d/1> (accessed on 1 January 2022).
41. Soghomonyan, S.; Chilingarian, A.; Khanikyants, Y. Dataset for Thunderstorm Ground Enhancements Terminated by Lightning Discharges, Mendeley Data, V1. 2021. Available online: <https://data.mendeley.com/datasets/p25bb7jrfp/1> (accessed on March 31, 1 February, 2022).
42. Chilingarian, A.; Hovsepyan, G.; Soghomonyan, S.; Zazyan, M.; Zelenyy, M. Structures of the intracloud electric field supporting origin of long-lasting thunderstorm ground enhancements. *Phys. Rev.* **2018**, *98*, 082001.

43. Chilingarian, A.; Chilingaryan, S.; Reymers, A. Atmospheric discharges and particle fluxes. *J. Geophys. Res. Space Phys.* **2015**, *120*, 5845–5853. <https://doi.org/10.1002/2015JA021259>.
44. Chilingarian, A.; Hovsepyan, G.; Elbekian, A.; Karapetyan, T.; Kozliner, L.; Martoian, H.; Sargsyan, B. Origin of enhanced gamma radiation in thunderclouds. *Phys. Rev. Res.* **2019**, *1*, 033167.
45. Shmatov, M.L. Possible detection of visible light and γ rays from a swarm of ball lightning. *Phys. Rev. E* **2020**, *102*, 013208. <https://doi.org/10.1103/PhysRevE.102.013208>.
46. Lowke, J.J.; Heil, W.; Tam, E.; Murphy, A.B. Murphy, Toward a theory of ball lightning occurring in houses and aircraft. *J. Atmos. Sol.–Terr. Phys.* **2021**, *214*, 105532.
47. Khaerdinov, N.S.; Dzhappuev, D.D.; Kanonidi, K.K.; Kudzhaev, A.U.; Kurennya, A.N.; Lidvansky, A.S.; Petkov, V.B.; Khaerdinov, M.N. Disturbance of a Glow in the Night Sky in Clear Weather at Middle Latitudes. *Bull. Russ. Acad. Sci. Phys.* **2021**, *85*, 1308–1310. <https://doi.org/10.3103/S1062873821110149>.